Diyala Journal of Engineering Sciences

Journal homepage: https://djes.info/index.php/djes

ISSN: 1999-8716 (Print); 2616-6909 (Online)

Experimental and Numerical Investigation of the Effects of Transverse Reinforcement and Shear Span on Shear Capacity in Reinforced Concrete Cantilever Beams

Othman Majeed Abdullah*, Aziz Ibrhim Abdulla and Wisam Amer Alus

Department of Civil Engineering, University of Tikrit, Tikrit, Iraq

ARTICLE INFO

Article history:

Received August 19, 2024
Revised October 19, 2024
Accepted October 23, 2024
Available online December 1, 2024

Keywords:
ABAQUS
Concrete
Finite elements
Rotation
Stirrups

ABSTRACT

This paper examines the impact of transverse reinforcement and shear span on the shear capacity of reinforced concrete (RC) cantilever beams through both experimental and numerical investigations. The experimental program included testing nine RC beams, each with dimensions of 200 × 300 × 1200 mm. The experimental results were compared with analytical predictions derived from empirical models based on the ACI 318-19 and British Standards (BS) codes.The findings reveal that stirrups significantly enhance shear strength, resulting in an increase in load-carrying capacity ranging from 16.6% to 32.7%, while ductility, as evidenced by increased rotation and curvature, improved by up to 260%. The stirrup spacings employed in the specimens were 75, 100, and 150 mm, with both reinforced and unreinforced specimens exhibiting shear failure.Increasing the shear span-to-depth ratio (a/d) from 2.44 to 3, while keeping the stirrup spacing at 75 mm, resulted in a 12.9% reduction in ultimate load capacity. When the stirrup spacing was increased to 100 mm, the ultimate load capacity experienced a further decline of 23.9%. All beams were analysed using the finite element software ABAQUS, with the finite element analysis (FEA) results closely aligning with the experimental outcomes, particularly in the load-deflection relationship and maximum load capacity. On average, the predicted ultimate load capacity from ABAQUS was 2.7% lower than the experimental results, while the average difference in deflection at ultimate loads between the experimental and numerical results was 7.54%.

1. Introduction

Understanding the mechanisms of shear failure and shear resistance is crucial in the analysis of reinforced concrete (RC) beams. Over the past two decades, extensive studies have been conducted to investigate the degradation of shear capacity and the contribution of concrete to the shear strength of RC members as a function of ductility demand [1-4].The experimental research has established a solid foundation for understanding the mechanics of shear transmission as well as for developing theories, models, and design code requirements. The shear strength of reinforced concrete (RC) members diminishes more rapidly than their flexural strength in regions where maximum shear and flexural forces are concentrated. Consequently, when designing new reinforced concrete buildings and assessing existing structures, it is crucial to account for this reduction in shear resistance [5]. For reinforced concrete beams with a large shear span-to-effective depth ratio (a/d), it is widely accepted that the total shear strength (V) is the sum of the shear strength provided by the concrete (Vc) and the shear strength contributed by the transverse reinforcement (Vs). Most current design codes [6-9] and the literature [10-12] apply a summation model, where the total

* Corresponding author.
E-mail address: engothman25@gmail.com
DOI: 10.24237/djes.2024.17406

shear strength is considered as the combined contribution of concrete and transverse reinforcement. However, the latest version of EC2 [13] departs from this approach by utilizing a variable-angle truss model for shear strength evaluation. Choi and Park (2010) [14] studied the reduction in shear strength resulting from inelastic flexural deformations. By applying a strain-based shear strength model, they developed an analytical method to estimate the reduced shear strength and deformation capacity of slender beams. Understanding stress flow and distribution within structural elements and investigating shear behaviour in RC beams, particularly in the plastic hinge region, heavily relies on the classification of reinforced concrete members into Bernoulli regions (B-regions) and discontinuity regions (D-regions). Traditional flexural theory can analyse B-regions, where stress distribution is uniform and follows Bernoulli's hypothesis, while a more nuanced approach is required for D-regions, characterized by disturbances in stress contours due to geometric or loading discontinuities, such as dapped ends, corners, corbels, and concentrated load zones [15, 16]. When it comes to RC beams with different stirrup spacings and shear span-to-effective depth ratios (a/d), the plastic hinge region acts as a link between these two types of regions. Beams with lower (a/d) ratios exhibit behaviour similar to D-regions, where shear forces dominate and stress flow is disrupted, while those with higher (a/d) ratios tend to resemble B-regions, where flexural forces are more critical. The role of stirrup spacing in influencing shear resistance is particularly significant in D-regions, where transverse reinforcement directly affects shear capacity. The focus of this study is on the separate effects of concrete (Vc) and transverse reinforcement (Vs) on shear resistance, especially in the plastic hinge region. This fills in a knowledge gap by looking at the complicated stress interactions in these areas. This analysis contributes to the development of more accurate predictive models and design codes, ensuring both B- and D-regions are adequately considered in structural design.

In many cases, a decrease in rotation capacity is caused by shear failure in areas lacking transverse reinforcement. This limitation complicates the redistribution of internal forces within the structural system. Even when members achieve their flexural strength and the reinforcement remains elastic, shear failures can still occur [17].

During the entire loading process, the variation of shear strength provided by the transverse reinforcement (Vs) relative to member deflection can be recorded [5]. The findings support the work of Priestley et al. [12] and Ruiz and Muttoni [18], demonstrating a correlation between the concrete shear strength (Vc) and member deformation, often associated with crack width. Additionally, authors [19] observed that not all stirrups crossing critical diagonal cracks (CDC) contribute to the maximum shear resistance in terms of transverse reinforcement shear stress. This aligns with the conclusions reached by Li et al. [20] through their analysis.

When relocating a concentrated load initially positioned at the free end of a beam (at 1 L) towards the fixed end by successive increments of a quarter of the span’s length (i.e., 0.75 L, 0.5 L, and 0.25 L), the structural responses are significantly influenced. Specifically, the load-carrying capacity of the beam increases as the deflection increases. This behaviour is attributed to the augmentation of negative moments (failure moments) resulting from the reduction in the lengths of their lever arms. Conversely, the torsional moments decrease due to the shortening of their torsional arms and the characteristic elliptical shape. [21]

Despite extensive research efforts, there remains a gap in the literature regarding the precise relationship between the shear capacity of reinforced concrete beams and the contribution of transverse reinforcement. Additionally, the role of concrete in resisting applied shear forces, particularly in relation to shear span to effective depth ratios, has not been comprehensively quantified. More research needs to be done on how the total shear resistance (V) and how it is distributed between the concrete (Vc) and the stirrups (Vs) during the loading process affect each other and how

they affect shear performance. For instance, research conducted by Arslan and Boloat (2013) found that a substantial portion of the concrete contributes to the shear strength of beams, with contributions ranging from 18% to 69%. Additionally, existing design codes, such as ACI 318-19 and BS 8110-1:1997, offer empirical equations for predicting shear strength. However, these equations may not sufficiently account for the effects of varying shear span-to-depth ratios (a/d) or the absence of stirrups. Consequently, this oversight can result in overly conservative designs, as these codes do not adequately capture the influence of these critical parameters on the shear behaviour of reinforced concrete (RC) beams. The development of flexural cracks within the plastic hinge region plays a critical role in determining the shear capacity of reinforced concrete beams. During seismic events, the oscillation of reinforced concrete structures induces the formation of multiple plastic hinges at critical points. These plastic hinges are significantly influenced by the presence and progression of flexural cracks, which, in turn, affect their shear capacity. Therefore, it is essential to investigate how flexural cracks impact the shear capacity of plastic hinges.

Furthermore, the extent of flexural cracking in plastic hinges is governed by the shear span-to-depth ratio (a/d). In this study, three different values of the a/d ratio are evaluated for each shear reinforcement ratio to assess their combined effect. This research aims to address existing gaps in the literature regarding the shear capacity of reinforced concrete (RC) beams, focusing on the interaction between transverse reinforcement (stirrups) and a/d ratios. The study examines how these factors influence load-bearing capacity, failure modes, deflection, and rotation.

Moreover, there is a shortage of comprehensive experimental data that explores the transition between shear and flexural failure modes across a wide range of a/d ratios, especially in cantilever beams commonly used in practical construction. To fill this gap, the study compares experimental results with predictions from design codes and finite element simulations using ABAQUS, aiming to enhance the accuracy of shear strength predictions.

The significance of this research lies in its thorough investigation of the interaction between concrete and transverse reinforcement in providing shear capacity under varying a/d ratios and stirrup spacing. It offers a detailed analysis of the shear behaviour of RC beams, including cases without shear reinforcement, and emphasizes the effect of stirrup spacing on crack development and load capacity. Additionally, the integration of experimental findings with numerical simulations using ABAQUS helps validate the numerical models, providing valuable insights for improving shear strength predictions.

2. Experimental program

2.1 Materials

The concrete mix used in this study consists of the same constituent materials as a conventional mix: cement, aggregate, and water. The cement used is Ordinary Portland Cement (OPC) Type I, manufactured by the Mass Cement Company in Iraq. It complies with the physical and chemical requirements outlined in the Iraqi Specifications (IQ.S. 5/1984) [22]. The fine aggregate is sand with a maximum particle size of 4.75 mm, sourced from the "Al Zawiyah" region. Crushed gravel, used as the coarse aggregate, is also obtained from the same region, with a maximum size of 12.5 mm. Both fine and coarse aggregates meet the requirements of the Iraqi Standard Specifications No. 45/1984 [23].

For steel reinforcement, the stirrups are made from 6 mm diameter bars with a yield stress of 530 MPa, while the longitudinal reinforcement consists of 16 mm diameter rebars with a yield stress of 600 MPa. The physical properties of the reinforcing bars were tested in accordance with ASTM A615M-16 standards [24]. Table 1 presents the detailed physical characteristics of the reinforcing bars.

2.2 Concrete Mix

The concrete mix was designed with a coarse aggregate size of 12.5 mm to achieve a target compressive strength of 25 MPa. A water-

to-cement ratio of 0.453 was used. The specimens were cured under damp burlap for 28 days. To evaluate the compressive strength, cylindrical samples measuring 300 mm in height and 150 mm in diameter were cast following ASTM C39M-14a standards [25]. After the 28-day curing period, the average compressive strength of three tested specimens was 25.9 MPa. The concrete mix used in this study consists of 378.22 kg/m³ of cement, 797 kg/m³ of fine aggregate, and 910 kg/m³ of coarse aggregate. The water content is 171.69 kg/m³, resulting in a water-to-cement (W/C) ratio of 0.453. This specific mix design ensures appropriate workability and strength characteristics for the reinforced concrete beams under investigation. Additionally, ASTM C 78-04 [26] conducted a flexural test on three prisms measuring $100 \times 100 \times 500$mm to examine the concrete's flexural strength. The modulus of rupture was measured to be 4.4 MPa. A simple support held each prism in place while it underwent two concentrated point loads. Moreover, the splitting tensile strength (*fct*) is measured by utilizing a standard concrete cylinder specimen measuring 150×300 mm in accordance with the guidelines provided by ASTM C496-96 [27]. The sample was subjected to a centrally applied load until it reached a failure point, resulting in a splitting tensile strength of 2.7 MPa.

Table 1: Characteristics of the reinforcing bars

Rebar	**Yield stress (*fy*) (MPa)**	**Ultimate stress (*fu*) (MPa)**	**Elongation %**
6 mm	530	549	4.7
16 mm	600	650	15.2

2.3 Configuration of Specimens

Nine cantilever-reinforced concrete (RC) beams were subjected to monotonic loading tests until failure. In practical construction, a rigid column typically supports the cantilever beam, with the point of zero moment occurring at the loading point of the specimens, as shown in Figure 1. All beams had a consistent width of 200 mm and a height of 300 mm. The shear span-to-effective depth ratios (a/d) used in this study were 2.44, 3, and 3.57. These ratios were chosen to induce various failure modes, with the lowest ratio marking the boundary between deep beam behaviour and slender beam behaviour (a/d > 2). The ratio was gradually increased toward h/2 (half the beam's height) to observe different failure mechanisms under the given design parameters.

The expected failure mode for each beam was predicted using an empirical equation from ACI 318-19. Three stirrup spacings 75, 100, and 150 mm were used for each shear span-to-effective depth ratio, as shown in Table 2. In the plastic hinge region, the top and bottom reinforcement consisted of 4ø16 bars and 2ø16 bars, respectively. Figure 2 provides the cross-sectional dimensions and reinforcement details of the beams. Failure modes were classified as S, C, and F, representing shear, combined, and flexural failure, respectively. The stirrup spacing was labelled as B1, B2, and B3, corresponding to 75 mm, 100 mm, and 150 mm, respectively. For example, a beam labelled B1S indicates an expected shear failure with a stirrup spacing of 75 mm.

2.4 Instrumentation and loading frame

Figure 3 illustrates a schematic representation of a typical cantilever specimen in the test setup. A 200-ton actuator was used to deliver a load with displacement control of 1 kN/Sec [28], Two linear variable displacement transducers (LVDTs) were installed at the top and bottom of the beam to measure displacements, from which the rotation at the plastic hinge region was calculated the plastic hinge length was calculated according to the equation of (Paulay & Priestley (1992). as illustrated below.

$$Lp=0.08L\times0.022fy\ dp \quad (1)$$

Where L is the shear span length, and dp is the diameter of the longitudinal rebar. A third LVDT was positioned at the free end of the beam to measure the total deflection at the free end . In addition, strain gauges were positioned to monitor the linear strain that developed in the concrete, shear reinforcement, and longitudinal reinforcement as the load was gradually applied.

3. Results and discussion

3.1. Load deflection relation

Figures 4 to 6 show the grouping of all beam specimens. The load-deflection responses are categorized into three groups based on the shear span-to-effective depth ratio (a/d) as shown in Table 3. In these tests, the (a/d) ratio is the primary variable, while the stirrup spacing is held constant. During the initial loading phase, the results demonstrate a clear linear relationship between the applied load and the deflection of the beams, indicating elastic behaviour. Variations in stirrup spacing 75 mm, 100 mm, and 150 mm significantly affect the deflection at the failure load. Beams with closer stirrup spacing exhibit reduced deflection at the ultimate load, underscoring the role of transverse reinforcement in controlling shear deformation and enhancing load-carrying capacity. An increase in the (a/d) ratio for the first group of beams (B1S, B1C, and B1F) from 2.44 to 3.0 and 3.57 resulted in a decrease in ultimate load capacity. This indicates that as the (a/d) ratio increases, the shear demand decreases, causing the beam to behave more flexural. Consequently, the deflection at similar load levels increases. Beam B1F, with the highest (a/d) ratio, experienced the greatest deflection due to its flexural failure mode. In contrast, beams B1S and B1C exhibited shear and combined failure modes, respectively. These results emphasize the importance of the (a/d) ratio in determining the transition from shear to flexural failure and highlight the influence of stirrup spacing on the beam's ultimate load and deflection behaviour.

In summary, increasing the (a/d) ratio in the first group of beams led to a reduction in ultimate load capacity while increasing deflection at comparable load levels. Beam B1F showed the highest deflection due to flexural failure, unlike B1S and B1C, which exhibited shear and combined failure modes. Figures 4 to 6 provide detailed insights into how stirrup spacing and the (a/d) ratio impact deflection, ultimate load capacity, and failure modes. All other beam groups exhibited similar trends, except for the third group, where different behaviour was observed. In the third group of beams, shear failure occurred due to the absence of shear reinforcement in the plastic hinge region. Initially, flexural cracks developed in the centre of the plastic hinge region. As loading progressed, shear cracks formed at an angle of approximately 45 degrees. With further increases in load, these cracks increased in size, ultimately contributing to the failure of the beam as shown in Figure 7. Beams with closely spaced stirrups exhibited a steeper descending slope in the load-deflection curve, indicating enhanced shear capacity and improved crack control. These beams showed higher initial stiffness and a smoother transition from elastic to plastic behaviour, achieving greater ultimate load and deflection before failure. Conversely, beams with widely spaced stirrups demonstrated reduced shear capacity, resulting in larger cracks, a flatter initial slope, and lower initial stiffness. This led to a less ductile response and more abrupt failure. The crack surfaces across the beams were smooth, underscoring the importance of adequate shear reinforcement in influencing the performance and failure modes of the beams.

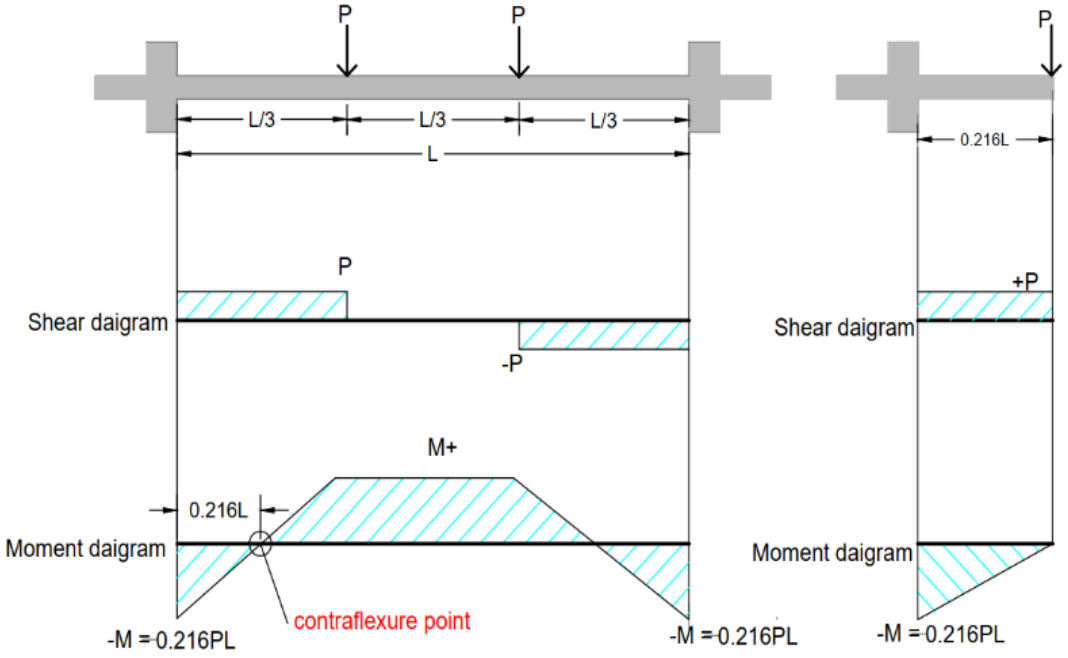

Figure 1. Shear force and bending moment diagrams of the experimental model.

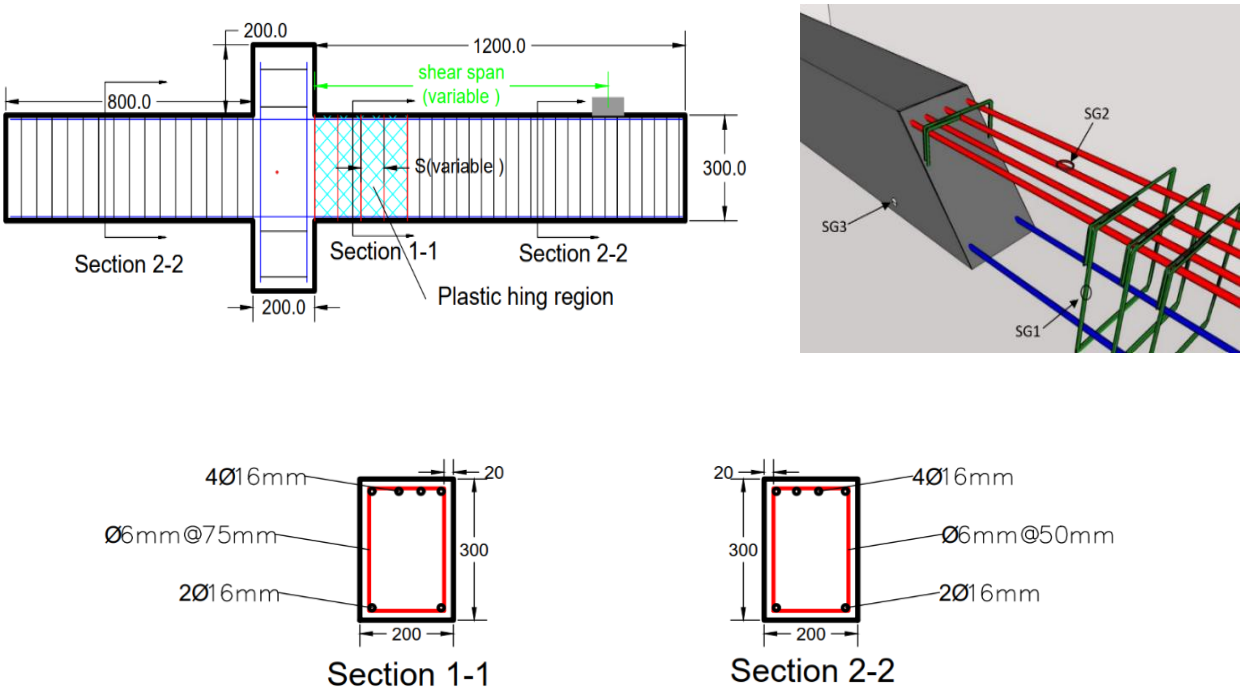

Figure 2. Beam details

Table 2: Characteristics of beams

#	Group no.	Beam symbol	spacing (mm)	Shear reinforcement Ratio (%)	shear span (mm)	(a/d)
1	**First group**	B1S	75	0.4	650	2,443
2		B1C	75	0.4	800	3
3		B1F	75	0.4	950	3.571
4	**Second group**	B2S	100	0.3	650s	2.443
5		B2C	100	0.3	800	3
6		B2F	100	0.3	950	3.571
7	**Third group**	B4S1	……..	……..	650	2,443
8		B4S2	……..	……..	800	3
9		B4S3	……..	……..	950	3.571

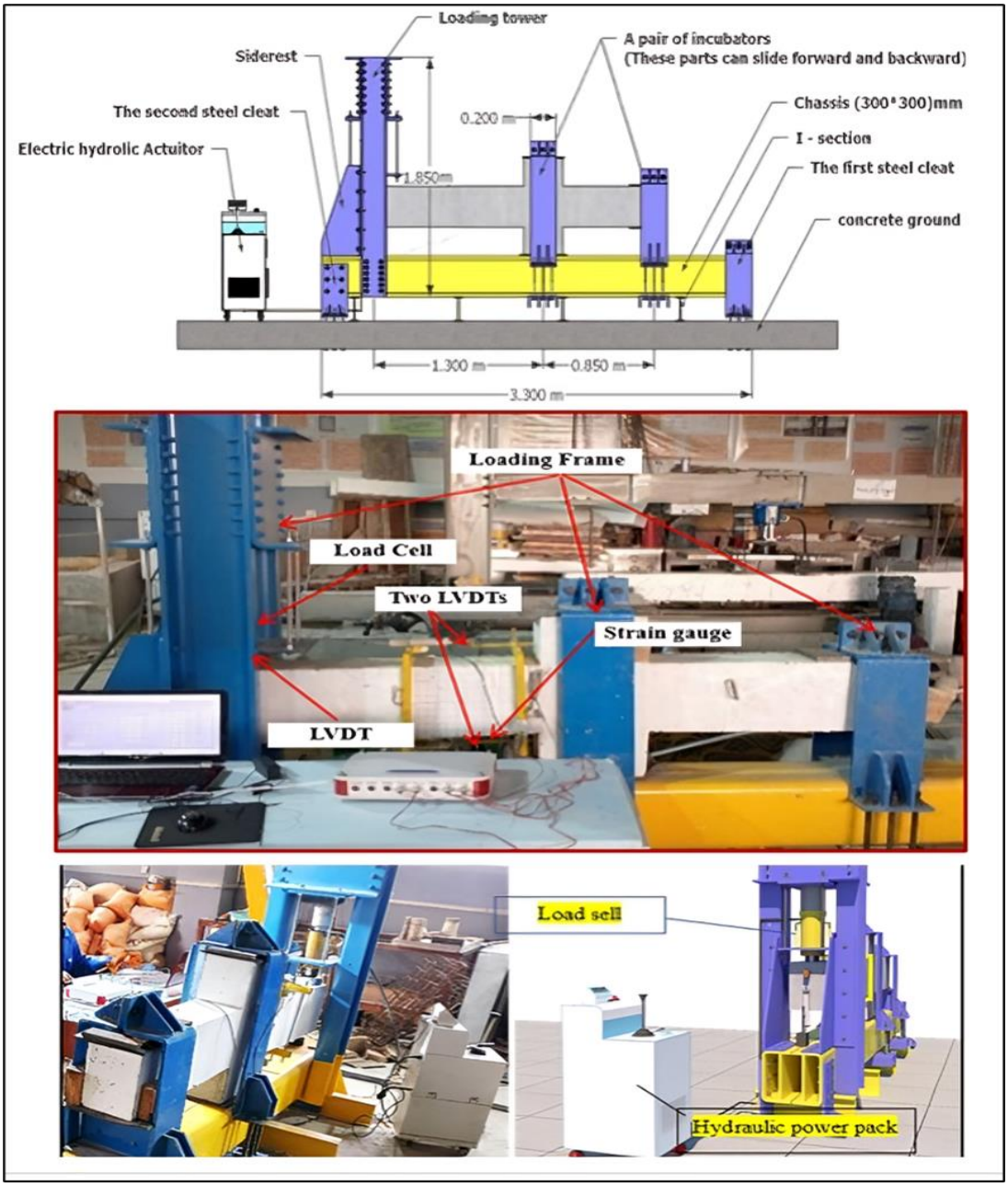

Figure 3. Loading frame and test set up

3.2. The shear strength of reinforced concrete members

In most of the current design codes, a superposition methodology has been adopted; the shear resistance of a RC member (V) consists of the contributions of (i) transverse reinforcement (Vs) and (ii) concrete (Vc). Shown in Figure 8, are the components of shear strength contributions around the critical diagonal crack (CDC). The equilibrium of the free body in the vertical direction results in equation (2).

$$V = V_c + V_s = \sum_1^n V_{sn} \quad (2)$$

Most shear design equations, including those in ACI 318-19 [30] and BS 8101:1997 [31], combine the effects of transverse reinforcement and concrete strength without considering whether flexural yield has occurred before shear failure. Table 4 presents the common empirical equations defining the contributions of steel and concrete in structural members

Guray Arslan et al. [32] and Biao Hu et al. [33] presented a method to determine the contributions of concrete and transverse reinforcement in resisting the shear force. These methods employ the following steps to determine the respective contributions of each component. The contributions of transverse reinforcement and concrete to shear force were calculated as follows:

- For each value of strain, the stress in the transverse reinforcement was computed from the stress-strain curve by iteration.
- The contribution of transverse reinforcement to the shear force was computed by multiplying the ratio of transverse reinforcement with the stress in the transverse reinforcement and cross-sectional area of the beam ($b_w d$)
- The contribution of concrete (Vc) to the shear force was computed by subtracting the average contribution of transverse reinforcement to the shear force from the shear force due to the applied load, as given in Equation (3).

$$Vu = V_c + V_s \quad (3)$$

Figure 9 presents the calculated variations in total shear strength (V), shear strength from transverse reinforcement (Vs), and concrete shear strength (Vc) for beams in the plastic hinge region. The stirrups absorb a minor fraction of the applied stress (Vc), contributing to the overall shear capacity of the beam by providing additional resistance against diagonal cracking, while specimen B1S absorbs the majority of the force before the first diagonal crack emerges. Concrete diagonal cracking is indicated by the difference between the V and Vc curves as well as the rise in Vs. Despite a very little slope, Vc keeps rising. The increased load is still supported by the transverse bars. Concrete and stirrups contribute to raising the load until it reaches maximum shear resistance. Before the diagonal cracking is created, specimen B2S behaves similarly to B1S. However, After the first crack occurred at a load of 44.3 kN, the contribution of Vc decreased slightly, marking the transition from linear to plastic behaviour. Following this, Vc gradually increased as the loading continued. Meanwhile, VS rise rapidly at the onset of the cracking process, reaching a value of 47.95 kN, followed by a curve with a steadily decreasing slope. This tendency is consistent with Priestley et al. [34] and Ruiz and Muttoni [35].

Table 5 provides a detailed comparison between the predicted concrete shear capacity (V_C) from the ACI Code, the experimentally determined concrete shear capacity (V_C), the shear reinforcement contribution (Vs), the ultimate load (Vu), and the failure modes for various reinforced concrete beams. According to the ACI Code, the predicted shear capacity (Vc) remains constant at 44.33 kN for all beams. However, the experimentally obtained concrete shear capacity V_C shows significant variation, with Beam B3S achieving the highest value of 152.7 kN and Beam B3C recording the lowest value of 46.258 kN. The ratio ($V_{c\,exp}/V_{c\,ACI}$ shows considerable increases, ranging from 3.36 in Beam B2S to 1.043 in Beam B3C. This suggests that the ACI Code may be more conservative

regarding the shear capacity, particularly in beams, where the experimental concrete shear capacity is more than three times the predicted value. The shear reinforcement contribution (Vs_{exp}) also varies, with beam B3C having the highest Vs of 86.652 kN, a 111% increase compared to beam B1C 41.027 kN. This indicates that beams with combined failure modes, such as B3C, rely more heavily on shear reinforcement. Beam B1S has the highest ultimate load (Vu) at 189.6 kN, while B3C has the lowest at 132.91 kN, indicating a 30% reduction. The ratio of (V_c/V_S) varies from 0.348 in B3C, indicating a strong reliance on reinforcement, to 0.873 in B3S, where concrete plays a more substantial role in load bearing. The failure modes also show that beams that fail in shear, like B3S, have higher Vc values, while beams that fail in combined, like B3C, have lower Vc and depend more on shear reinforcement.

Table 6 presents a comparison between the experimentally measured shear strengths of reinforced concrete beams and the theoretical predictions based on ACI 318-19 and BS 8110-1. The differences are expressed as the ratios of the theoretical to experimental values (Vc-Theo/Vc-test). For Beam B1S, the experimental shear capacity is 141.64 kN, with ACI and BS ratios of 0.306 and 0.3, respectively. These ratios indicate that both codes predict approximately 30% of the actual capacity, reflecting a 70% conservative estimation. Similarly, for Beam B1C, which has an experimental capacity of 126.89 kN, the ACI and BS ratios are 0.345 and 0.34, showing that both codes estimate around 34–35% of the actual capacity—an underestimation of 65%. Beam B2S, with an experimental capacity of 148.93 kN, has ACI and BS ratios of 0.296 and 0.29, meaning the codes predict roughly 30% of the actual capacity, resulting in a 70% conservative estimate. Beam B2C, with a test capacity of 106.82 kN, shows slightly higher ACI and BS ratios of 0.405 and 0.4, indicating that these codes predict about 40% of the actual capacity, reflecting a 60% reduction. The minimal differences between the ACI and BS predictions suggest that both codes exhibit similar levels of conservatism. Across all beams, the design codes consistently produce conservative shear capacity estimates, with reductions ranging from 60% to 70%. However, the discrepancy is somewhat lower for Beam B2C, where the codes predict around 40% of the experimental capacity.

The points at which the shear force (V) curve diverges from the concrete shear capacity (Vc) curve signify the contribution of the stirrups (Vs) to the overall shear resistance. Initially, the concrete shear capacity (Vc) increases at a relatively shallow slope, indicating that the concrete provides limited shear resistance before the onset of cracking. Once cracking occurs, the stirrups assume a more critical role in resisting shear, thereby enhancing the overall shear capacity of the beam. As the load continues to increase, the stirrups effectively resist additional shear forces, further improving the beam's shear performance. The emergence of diagonal cracks marks a crucial transition in the beam's response. Following the initial appearance of these cracks, the concrete shear capacity (Vc) experiences a decline at the fracture point but gradually recovers until the beam ultimately fails. Conversely, the shear resistance provided by the stirrups (Vs) increases sharply at the onset of cracking, although this rate of increase progressively diminishes over time. This observed behavior is consistent with the findings of Priestley et al. [34] and Ruiz and Muttoni [35]. In this analysis, the contribution of concrete to the shear capacity is determined by subtracting the shear force resisted by the stirrups (Vs) from the total applied shear force (V). The shear strength provided by the stirrups is calculated by multiplying the strain in each stirrup by its modulus of elasticity and the effective cross-sectional area (bw*d), as detailed in section 3.2. This approach allows for the quantification of the relative contributions of both concrete and stirrups to the overall shear capacity of the beam.

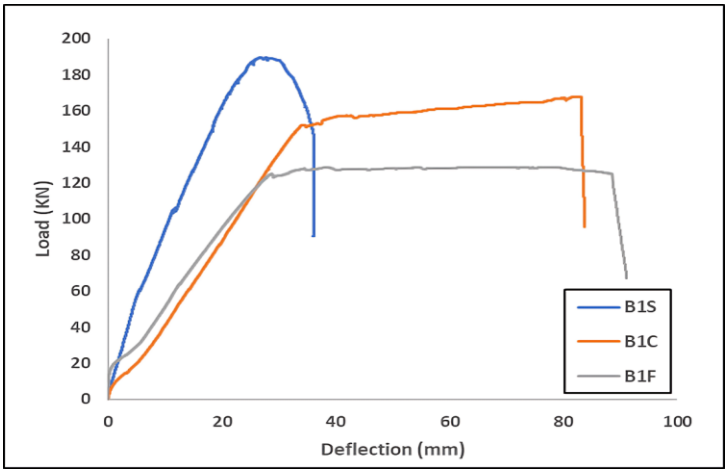

Figure 4. Load-deflection curve for first group

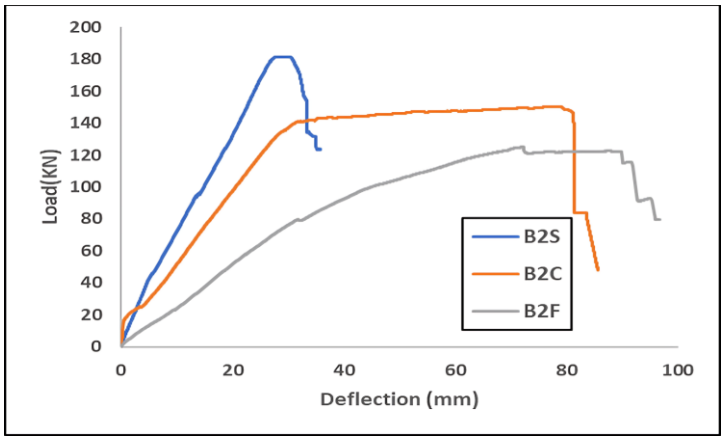

Figure 5. Load-deflection curve for second group

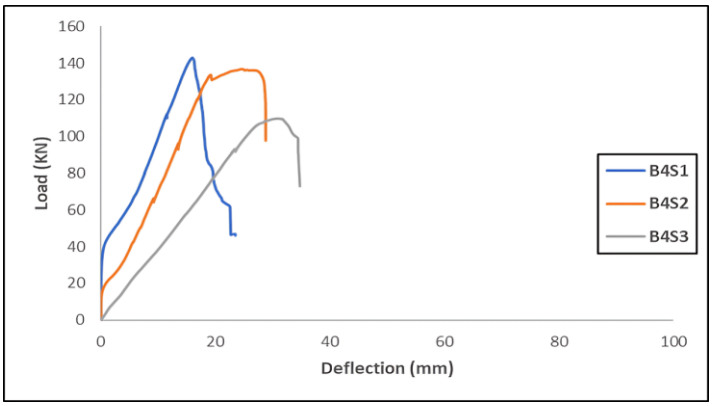

Figure 6. Load-deflection curve for third group

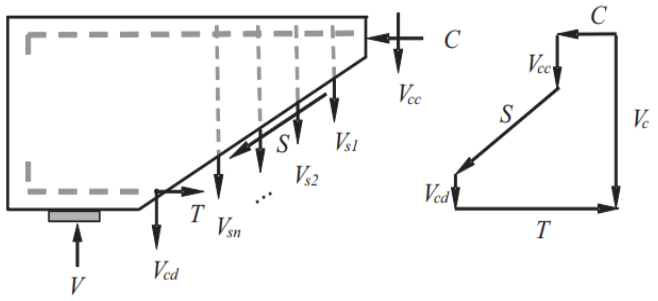

Figure 7. Components of shear resistance (Hu, and Wu, 2017)

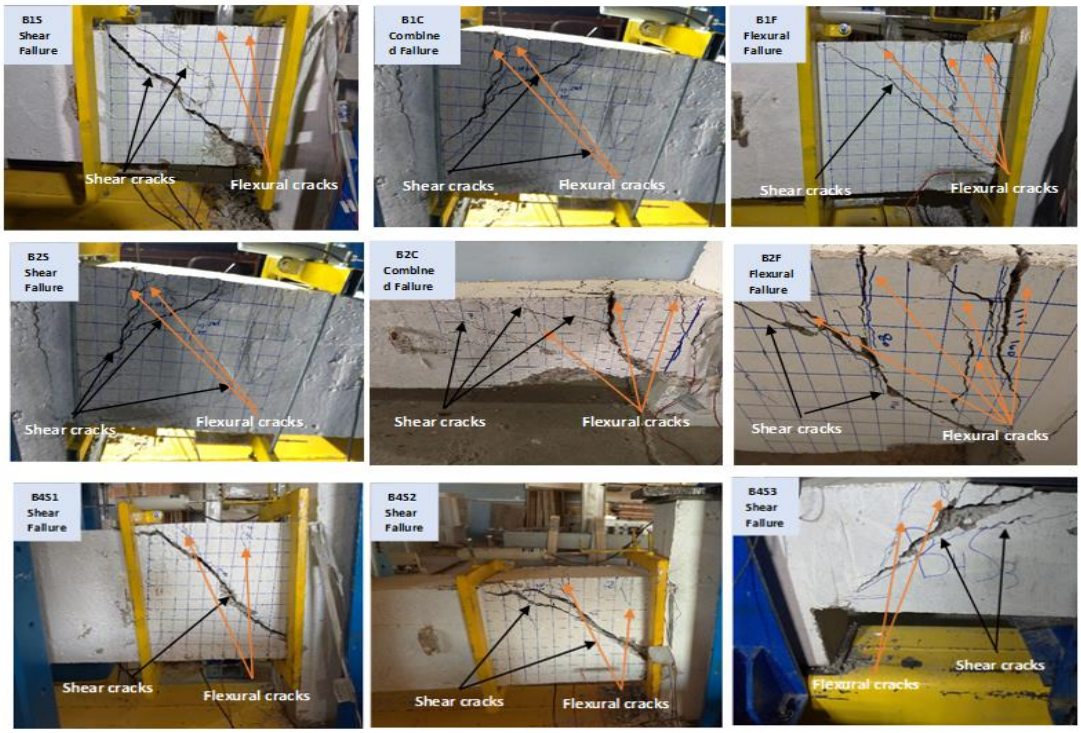

Figure 8. Crack pattern for tested beams

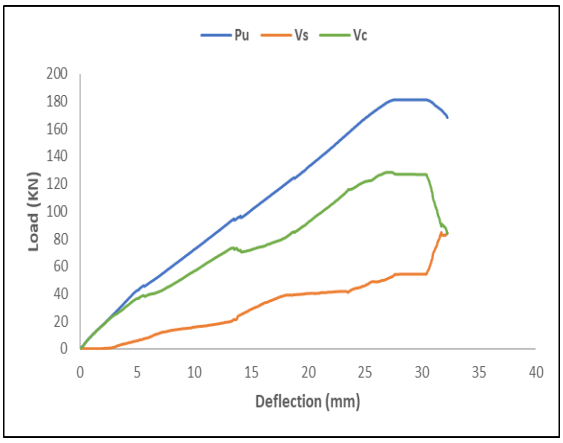

a) B1S

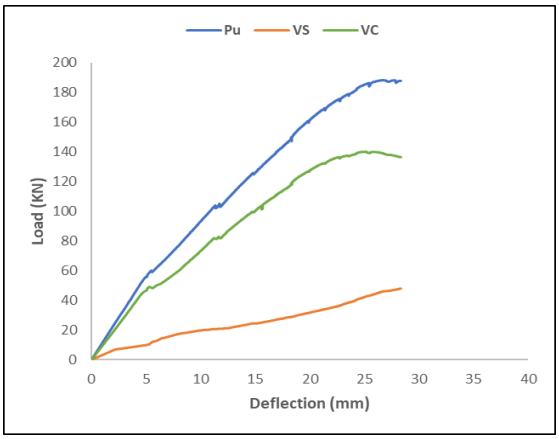

b) B2S

Figure 9. Contribution of concrete and transverse reinforcement to shear force for B1S and B2S

Table 3: Ultimate load and deflection at free end

Symbol	a/d	Pu (KN)	Deflection (mm)	Mode failure
B1S	2.44	189.6	26.816	Shear failure
B1C	3	167.92	82.94	Combined failure
B1F	3.571	128.16	80.2	Flexural failure
B2S	2.44	186.034	27.622	Shear failure
B2C	3	150.14	77.61	Combined failure
B2F	3.571	124.97	72.223	Flexural failure
B4S1	2.44	142.87	15.952	Shear failure
B4S2	3	136.681	24.64072	Shear failure
B4S3	3.571	109.868	31.0095	Shear failure

Table 4: Shear design provisions for reinforced concrete according to ACI-Code 318-19 and BS8110 codes

ACI 318-19	Either of: (If Av≥ Av min)	$Vc = \left[0.17\lambda\lambda s\sqrt{f}c + \frac{Nu}{6Ag}\right] bw.d$ $Vc = \left[0.66\lambda(\rho)^{\frac{1}{3}}\sqrt{f}c + \frac{Nu}{6Ag}\right] bw.d$	$Vs = \frac{Av.fyv.d}{S}$	$Vu = VC + VS$	Notes: 1- The axial load, Nu, is positive when it causes compression and negative when it causes tension. 2- The value of Vc must not be less than zero. $\lambda s = \sqrt{\frac{2}{1+0.00394d}} \leq 1$ $\lambda = 1\ for\ Normal.Con.$
BS811۰: 1997	$Vc = \left[\frac{0.79}{\lambda m}\left(\frac{100As}{bvd}\right)^{(1/3)}\left(\frac{400}{d}\right)^{(1/4)}\left(\frac{fcu}{25}\right)^{(1/3)}\right] * bw.d$		$Vs = \frac{0.95\ Av.fyv.d}{S}$		For a/d ≥ 2 $\lambda m = 1.25$ $\left(\frac{100As}{bwd}\right)$ *should not be taken as greater than* 3 $\left(\frac{400}{d}\right)$ *should not be taken as less than* 1

Whear: -
Vc: concrete shear strength at failure
Vs: the shear resistance provided by shear reinforcement,
Av: the area of shear reinforcement within a distance of S (mm).
fy: the transverse reinforcement yields strength (MPa).
bw: beam width(mm).
d: is the effective depth(mm).
fc: the concrete's compressive strength (MPa)

3.4 Shear strength of beams without stirrups

The American Concrete Institute's ACI 318M-14 [36] provides two equations for calculating the shear strength of beams without shear reinforcement, either for combined flexure and shear or for shear alone. The first equation determines the basic shear strength, while the second equation offers a simplified approximation commonly used in design practice. The simplified design equation, which depends solely on the compressive strength of the concrete, does not account for load effects or size influences.

$$Vc = 0.17\sqrt{f}cbw.d \quad (4)$$

On the other hand, the British standard BS 8110-1:1997 indicates that the shear strength values increase when d is less than 400 mm, as indicated by the equations in Table 4.

Table. 9 show the comparison of beams with and without stirrups. In reinforced concrete beams without stirrups, the dowel action is one of the important Parameters in resisting the internal shear force. To predict the dowel force (Vd) in beams, the equation presented by Houde and Mirza [37] was used as follows:

$$V_d = 37b_n\sqrt[3]{f}c \quad (5)$$

$$V_u = V_C + V_d \quad (6)$$

for beams without shear reinforcement
Where b_n is the net width of the beams.

Dowel action primarily depends on the material properties of concrete and steel reinforcement, such as their yield strength, modulus of elasticity, and bonding characteristics. These properties are intrinsic to the materials and remain constant, independent of the applied load. As a result, conventional equations for dowel action reflect this independence by focusing on material properties rather than load effects [38]. The ACI 318-19 and BS 8110 design codes assign constant shear strength values as the shear span-to-depth ratio (a/d) increases. Table 7 presents shear strength data for beams with a constant effective depth of 266 mm and varying (a/d) ratios. The experimental shear strengths significantly exceed the values predicted by both codes. For example, Beam B4S1, with an (a/d) ratio of 2.443, has an experimental shear strength of 2.36 MPa approximately 274% of the BS 8110 value and 291% of the ACI 318-19 value. Similarly, Beam B4S2, with an (a/d) ratio of 3, exhibits a shear strength of 2.243 MPa, representing about 260% of the BS 8110 prediction and 276% of the ACI 318-19 value. For Beam B4S3, which has an (a/d) ratio of

3.571, the measured shear strength is 1.739 MPa—202% of the BS 8110 prediction and 214% of the ACI 318-19 value. These significant margins indicate that the experimental shear strengths are substantially higher than the theoretical values provided by the design codes. The discrepancy between the measured and predicted shear strengths becomes more pronounced at higher (a/d) ratios, where the experimental shear strength decreases, demonstrating a notable deviation from theoretical predictions. This suggests that both ACI 318-19 and BS 8110 tend to be overly conservative, particularly for beams with high (a/d) ratios. The findings imply that current design standards may not accurately account for how increasing shear span affects the concrete's shear capacity (Vc). The experimental results highlight a strong relationship between the (a/d) ratio, shear strength, and rotation capacity. As the (a/d) ratio increases, the rotation capacity decreases, indicating reduced ductility. This behaviour aligns with the shift in failure modes, transitioning from shear failure at low (a/d) ratios to flexural failure at higher (a/d) ratios. In conclusion, while the ACI 318-19 and BS 8110 formulas provide reliable predictions for beams with low (a/d) ratios, their accuracy diminishes as the (a/d) ratio increases.

3.5 The effect of the presence and absence of stirrups on the behaviour of beams

A comparison between the results from the first group (B1S, B1C, and B1F) and the third group (B4S1, B4S2, and B4S3) highlights key differences in failure modes. All beams in the third group failed due to shear, regardless of the shear span-to-depth (a/d) ratio. In contrast, the failure mode in the first group varied with the (a/d) ratio. As the (a/d) ratio increased from 2.443 to 3.571, the failure mode transitioned from shear failure to combined failure and eventually to flexural failure.

Stirrups played a significant role in enhancing the shear strength of the beams. Their presence increased the shear capacity by 16.6% to 32.7%, as illustrated in Figure 10. Stirrups also improved the rotational capacity within the plastic hinge region, increasing rotation by 69.18%, 115.11%, and 260.50% for (a/d) ratios of 2.443, 3, and 3.571, respectively. Additionally, curvature ductility improved by 78.83%, 165.08%, and 251.42% for the same (a/d) values as shown in Figure 11. The effect of stirrups on shear resistance (Vs) was examined using two approaches. The first approach involved calculating Vs from the stress-strain curve [32], while the second compared the shear strength of beams with and without stirrups under identical experimental conditions, focusing on the (a/d) ratio. At lower (a/d) ratios, both methods produced similar Vs values. However, as the (a/d) ratio reached 3, the Vs calculated from the stress-strain curve was 31.3% higher than that obtained from the second method. At an (a/d) ratio of 3.571, the difference became more pronounced, with the stress-strain curve method yielding a value 76.25% higher.

The presence or absence of stirrups significantly influenced the behaviour of reinforced concrete (RC) beams in terms of shear capacity, failure modes, and ductility. Beams with stirrups (B1S, B1C, and B1F) demonstrated enhanced shear resistance, especially at lower (a/d) ratios, where stirrups delayed or prevented brittle shear failure. For instance, B1S (a/d = 2.443) experienced shear failure at 189.6 kN. As the (a/d) ratio increased to 3, B1C exhibited combined shear and flexural failure at 167.92 kN. At an (a/d) ratio of 3.571, B1F failed in flexure at 128.16 kN. This progression indicates that as beams become more slender, flexural failure becomes dominant, though the presence of stirrups still allows for higher load capacities and improved ductility.

In contrast, beams without stirrups (B4S1, B4S2, and B4S3) exhibited lower shear capacities and failed in shear regardless of the (a/d) ratio. B4S1 (a/d = 2.443) failed at 142.87 kN, while B4S3 (a/d = 3.571) failed at 109.86 kN, highlighting that the absence of stirrups leads to premature shear failure. The load capacity ratio between beams with and without stirrups emphasizes the contribution of transverse reinforcement to shear resistance. For example, B1S can carry approximately 33% more load than B4S1 before failure. Overall, the analysis demonstrates that stirrups are essential

for improving both shear capacity and ductility, particularly at lower (a/d) ratios. Conversely, their absence results in a significant reduction in strength, underscoring the importance of transverse reinforcement in RC beam design.

4. Numerical analysis

ABAQUS provides two constitutive models for concrete: concrete-damaged plasticity (CDP) and concrete-smeared cracking (CSC). The CDP model is preferred due to its stability and is commonly used to analyse the mechanical behaviour of reinforced concrete beams under different loading conditions. The CDP model requires five parameters:

- Eccentricity (ε): Defines the asymptote of the flow potential, with a default value of 0.1.
- Viscosity parameter: Represents the relaxation time, defaulting to zero in ABAQUS.
- Yield surface: Based on the stress invariants in tensile and compressive meridians, with a default kc value of 0.667.
- Equiaxial compressive yield stress: Ratio of initial uniaxial
- stresses, with a default value of 1.16.
- Dilation angle (ψ): Defines plastic potential inclination, ranging from 0 to 56 degrees. A 30-degree dilation angle was used.

Table 8 presents the values for the CDP model, derived from experimental control specimen tests for each concrete strength. [39], modelling capabilities of ABAQUS [40] allow for accurate simulation of impact loading on reinforced concrete structures. A mesh with varying size was used to construct the three-dimensional finite element models. It is well understood that the number of elements plays a crucial role in determining the computation time and the accuracy of analysis results. Thus, the model is built using elements of different sizes to strike a balance between computation time and accuracy.

Table 5: Shear strength of beams

Beam	$\mathbf{Vc\ (ACICode)\ (kN)}$	$\boldsymbol{Vc^n}$ **(kN)**	$\frac{\mathbf{Vc^a}}{\mathbf{Vc(ACI\ Code)}}$	$\boldsymbol{Vs^m}$ **(kN)**	$\boldsymbol{Vu}$ **(kN)**	$\frac{\boldsymbol{Vc}}{\boldsymbol{Vu}}$	**Mode of Failure**
B1S	44.33	141.640	3.195	47.957	189.60	0.747	Shear Failure
B1C	44.33	126.898	2.863	41.027	167.925	0.756	Combined Failure
B2S	44.33	148.933	3.360	32.255	181.188	0.822	Shear Failure
B2C	44.33	106.820	2.410	43.320	150.140	0.711	Combined Failure
B3S	44.33	152.7	3.185	22.055	174.760	0.873	Shear Failure
B3C	44.33	46.258	1.043	86.652	132.910	0.348	Combined Failure

$\boldsymbol{Vc^n}$ Contribution of concrete to shear strength.
$\boldsymbol{Vs^m}$ Contribution of transverse reinforcement to shear strength.

Table 6: Comparison of shear strength components.

Beam	Test (kN)	ACI 318-19	BS 8110-1
	Vc	$Vc\text{-}Theo/Vc\text{-}test$	$Vc\text{-}Theo/Vc\text{-}test$
B1S	141.64	0.306	0.3
B1C	126.89	0.345	0.34
B2S	148.93	0.296	0.29
B2C	106.82	0.405	0.4

Table 7: Comparison of Shear Capacity Formulations for Beams with and without Stirrups

Beam	$\rho t(\%)$	$\rho v(\%)$	$S(mm)$	a/d	$Vd(kN)$	$Vu(kN)$	f_v BS8110 (MPa)	f_v ACI-318-19 (MPa)	f_v $exp.$ (MPa)
B1S	1.44	0.377	75	2.44	……..	189.6	0.798	0.814	2.662
B1C	1.44	0.377	75	3	……..	167.92	0.81	0.822	2.36
B1F	1.44	0.282	100	3.571	……..	128.16	0.823	0.831	2.4
B4S1	1.44	-----	-----	2.44	21.63	142.87	0.862	0.812	2.36
B4S2	1.44	-----	-----	3	21.63	136.68	0.862	0.812	2.243
B4S3	1.44	-----	-----	3.571	21.63	109.86	0.862	0.812	1.739

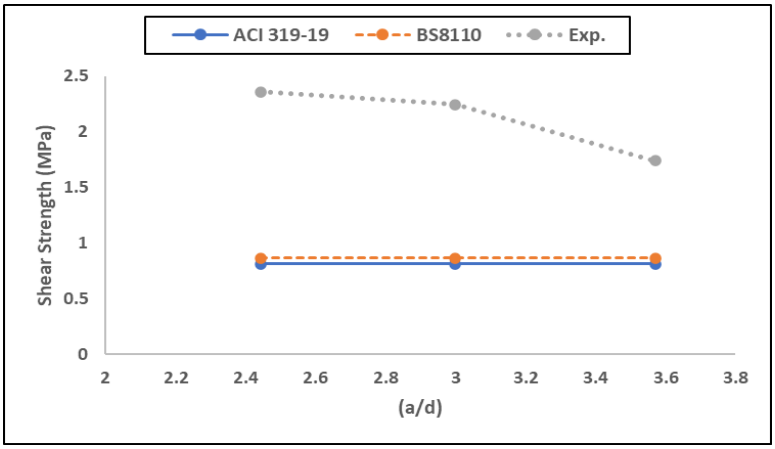

Figure 10. Impact of shear span-to-dept ratio on shear strength in beams with and without stirrups

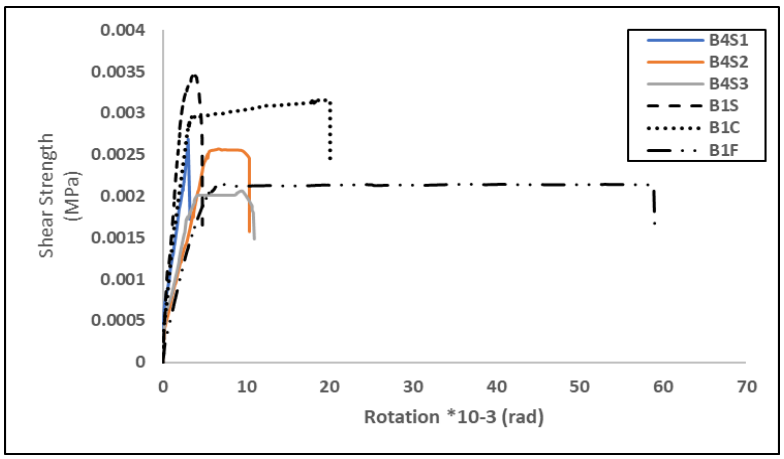

Figure 11. The shear strength versus rotation for the different methods results

In ABAQUS, the T3D2 element was utilized for modelling the reinforced material, while the C3D8R element was selected for the concrete. The reinforcement was embedded within the concrete element to simulate the bonding interaction between the two materials. The finite element model was constructed with careful meshing. As illustrated in Figure 12, the diameters of the transverse reinforcement stirrups and longitudinal reinforcing bars were both 20 mm, while the concrete elements were modelled as cubic elements measuring 15 mm on each side. The parameters for the concrete damaged plasticity model used in ABAQUS are presented in Table 8.

Additionally, the simulation of contact surfaces posed a challenge in the modelling procedure. To ensure an adequate bond between the reinforcement steel bars and the concrete, the reinforcement was designed appropriately,

and the stirrups were modelled accurately, utilizing the "embedded region" option in ABAQUS. For the interaction between the concrete and the loading plates in the analysis, the contact type was defined as "tie." Conversely, the interaction between the concrete and the supports was modelled using a "penalty" friction approach, with a friction coefficient set at 0.6 [40].

4.1 Finite Element Analysis Results

The difference between the load-midspan deflection response from the FE analysis and the results of the experimental tests is shown in Figures 13 to 15.

Table 8 : Damaged plasticity parameters

Plasticity	Value
Dilation angle	36
Eccentricity	0.1
fb0/fc0	1.16
K	0.6667
Viscosity parameter	0
Density of concert	$\mathbf{2.4 \times 10{-}6}$N/mm^3
Density of steel	$\mathbf{7.65 \times 10{-}5}$N/mm^3
Poisson's ratio of concrete	0.2
Poisson's ratio of steel	0.3
Concrete strength	C25

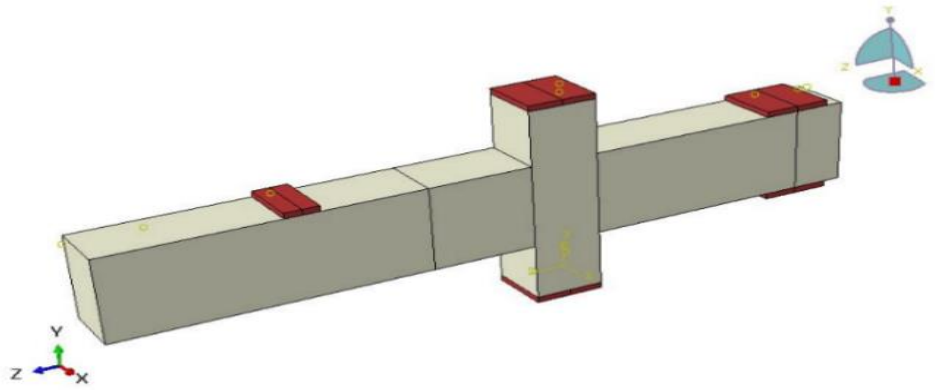

a)

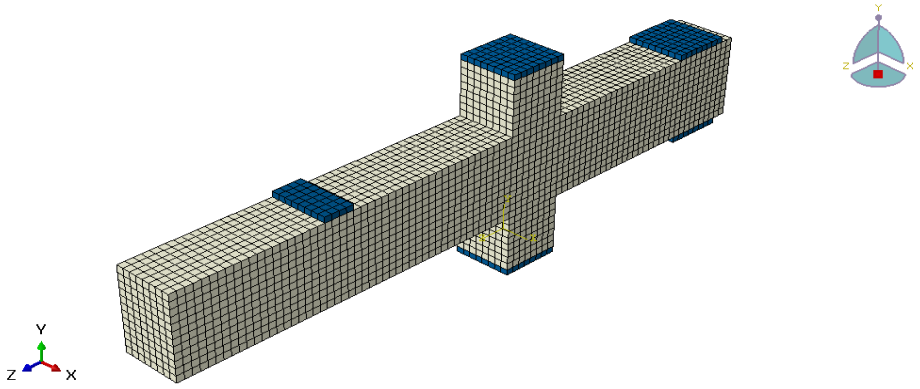

b)

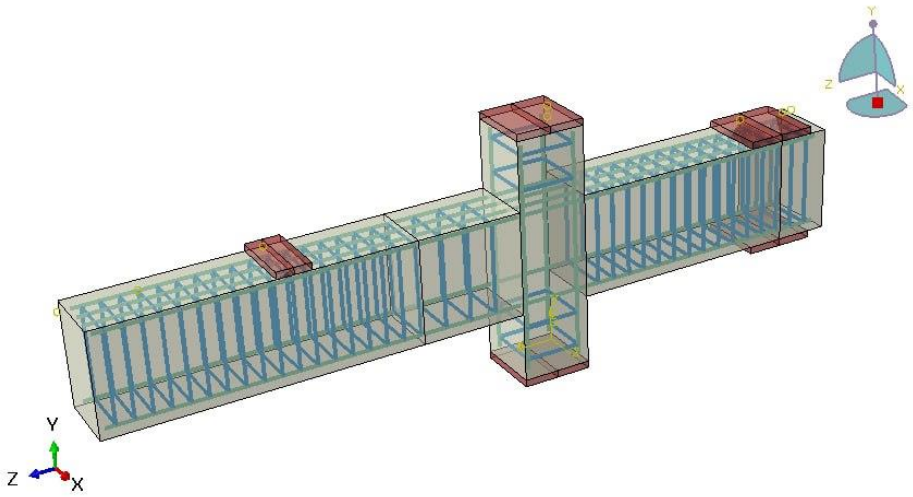

c)

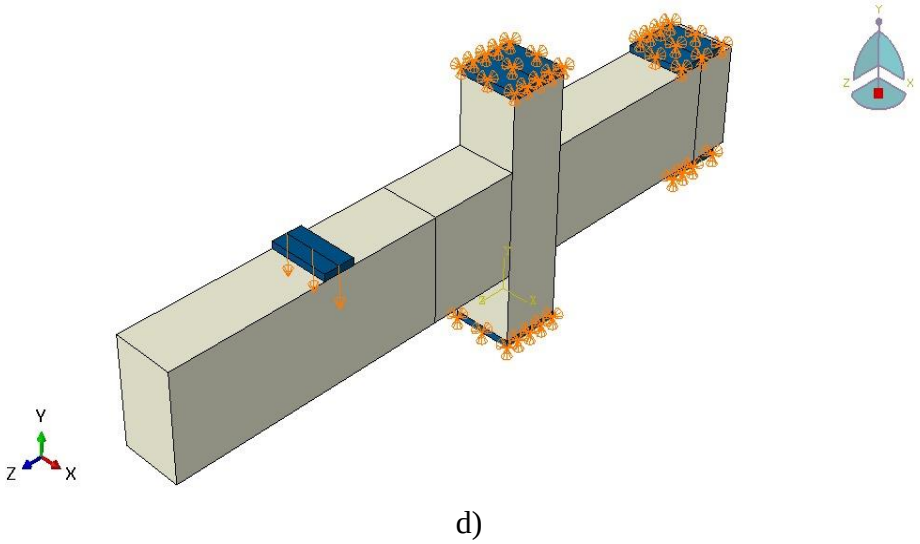

d)

Figure 12. (A) Loading and constraints, (B) Meshing of the beam., (C) Interaction of the Reinforced Concrete Beam with Its Surroundings, and (D) Boundary conditions

Table 9: Summary of experimental and finite element analysis results for all tested beams

Symbol	a/d	Pu (KN)		Exp/FE Ultimate load ratio	Deflection (mm)		Exp/FE Deflection ratio	Mode of Failure
		Exp.	FE		Exp.	FE		
B1S	2.44	189.6	194.882	1.027	26.816	30.8168	0.87	S. F
B1C	3	167.92	170.575	0.984	82.94	79.8043	1.039	C.F
B1F	3.571	128.16	136.828	0.937	80.2	65.2439	1.229	F. F
B2S	2.44	186.034	177.018	1.051	27.622	27.416	1.008	S. F
B2C	3	150.14	162.791	0.922	77.61	70.3077	1.104	C.F
B2F	3.571	124.97	132.987	0.940	72.223	72.1228	1.001	F. F
B4S1	2.44	142.87	152.834	0.935	15.952	15.2729	1.044	S. S
B4S2	3	136.681	139.066	0.983	24.64072	24.8848	0.990	S. S
B4S3	3.571	109.868	114.741	0.958	31.0095	31.538	0.983	S. S

The predictions made by the finite element analysis demonstrate a high degree of accuracy, closely aligning with the results obtained from the experimental tests. On average, the ultimate load capacity measured experimentally was slightly lower than that predicted by the ABAQUS software. At maximum loads, the average deflection difference between the theoretical predictions and actual measurements was found to be 7.54%. The failure modes of the reinforced concrete beams were effectively represented by the constitutive models used in the analysis. Table 9 presents the ultimate loads and maximum displacements at failure. The discrepancies observed between the experimental and numerical results can be attributed to the approximations inherent in the finite element method (FEM), primarily due to the following factors:

1. Simplifications in the material modelling of both concrete and steel.
2. Inherent approximations within the finite element technique.
3. This numerical analysis applies approximations in the integration function.
4. The method of solving the nonlinear system of equations introduces an approximation.

Across the three groups, it is evident that while the finite element (FE) model generally provides reliable predictions for ultimate loads and deflections, discrepancies are more pronounced in flexural and combined failure modes.

In the first group, the ultimate load ratios indicate that Beam B1S exhibited effective shear resistance. However, Beam B1C demonstrated a slight underestimation by the FE model in the combined failure mode, and Beam B1F highlighted potential shortcomings in modelling flexural behaviour, particularly due to its greater deflection. The ultimate load ratio for Beam B1F, at 0.937, shows a noticeable deviation from the predicted values, suggesting possible issues in the modelling of flexural behaviour. The higher deflection ratio of 1.229 indicates that the experimental beam was more flexible or ductile than expected, implying that the FE model might not fully capture the beam's flexural performance in this setup. The second group revealed that the shear failure beam B2S performed slightly better than predicted, while Beam B2C exhibited a conservative FE prediction for combined failure, emphasizing the challenges in accurately modelling such complex interactions. In contrast, Beam B2F aligned closely with experimental findings for deflection, indicating improved calibration in flexural behaviour. The ultimate load ratio for Beam B2C, at 0.922, indicates that the FE model provided a more conservative prediction, suggesting it may not fully account for the combined effects of shear and flexural forces in the beam's failure. The deflection ratio of 1.104 reveals that the beam deflected more than anticipated, highlighting the challenges in accurately predicting the behaviour of beams under combined loading conditions.

The third group displayed a consistent pattern, where the beams that failed due to shear performed slightly less than expected based on the predictions. The small differences in deflection suggest that modelling shear performance could be improved. Figures 23 to 25 compare the failure modes observed during testing with those predicted by the numerical analysis. The numerical models successfully predicted the diagonal tension cracking observed in the experiments. Additionally, the finite element analysis revealed diagonal cracks in all the beams, which were caused by tension splitting in the plastic hinge region. These figures illustrate the close correspondence between the numerical predictions and the experimental results.

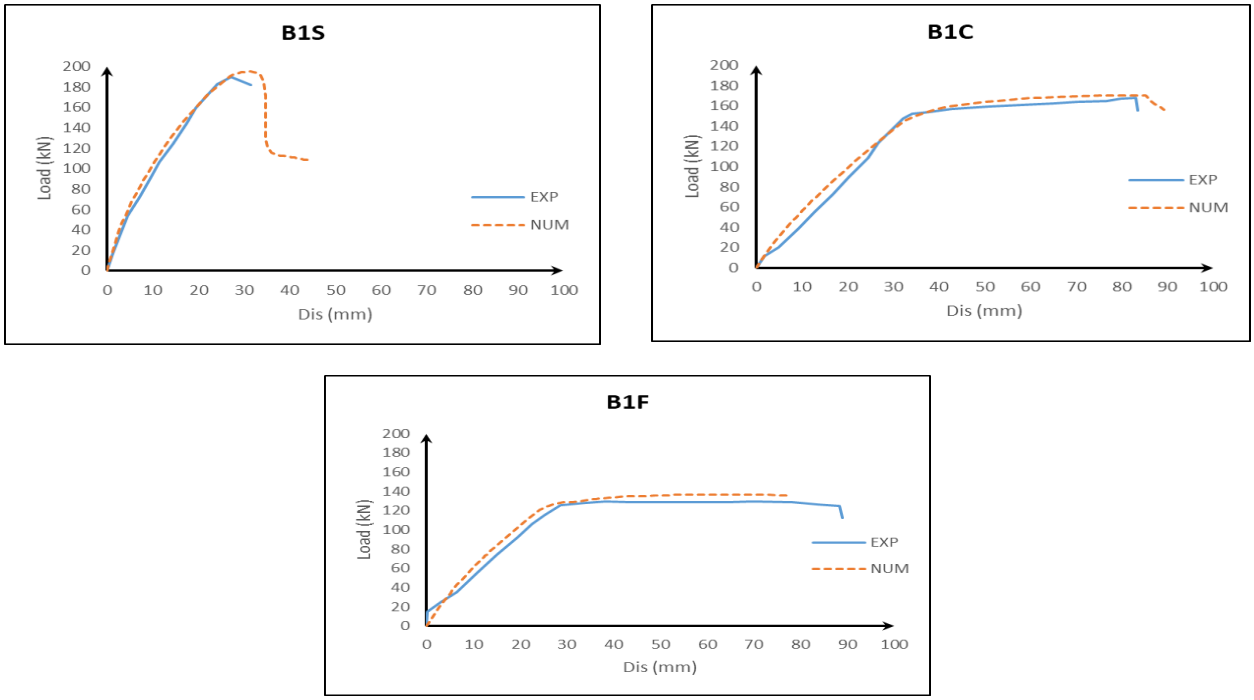

Figure 13. The load-deflection responses for first group both numerical and experimental

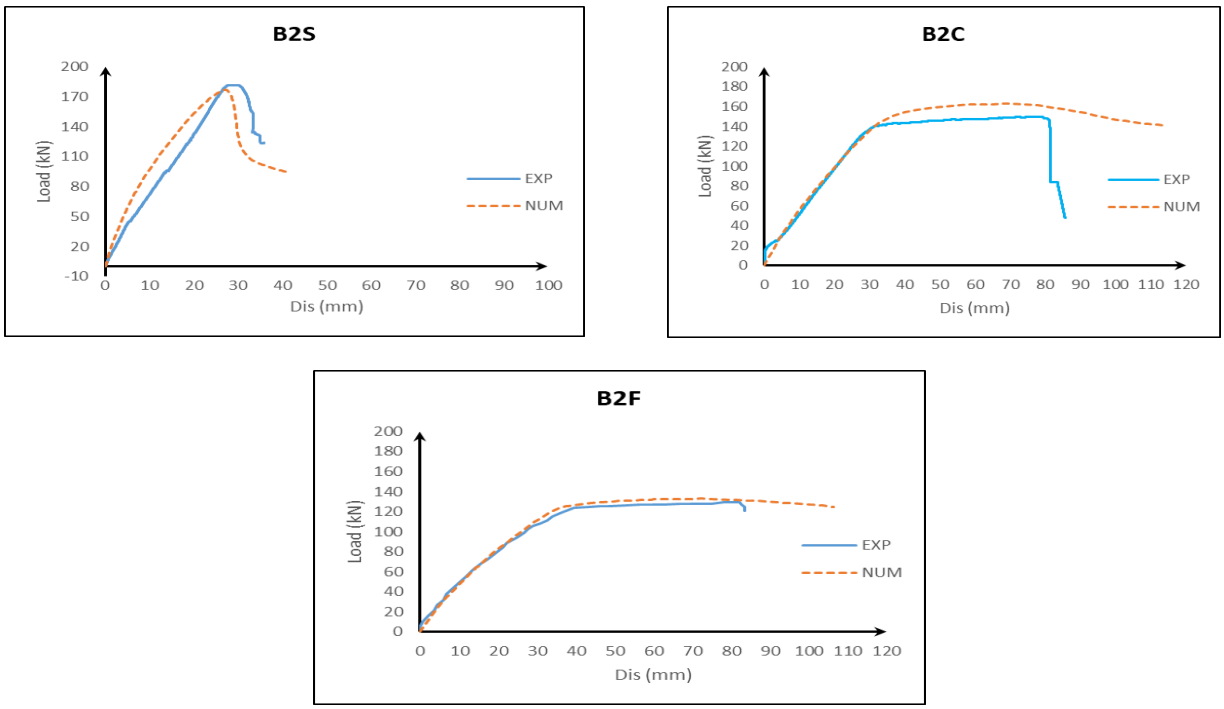

Figure 14. The load-deflection responses for second group both numerical and experimental

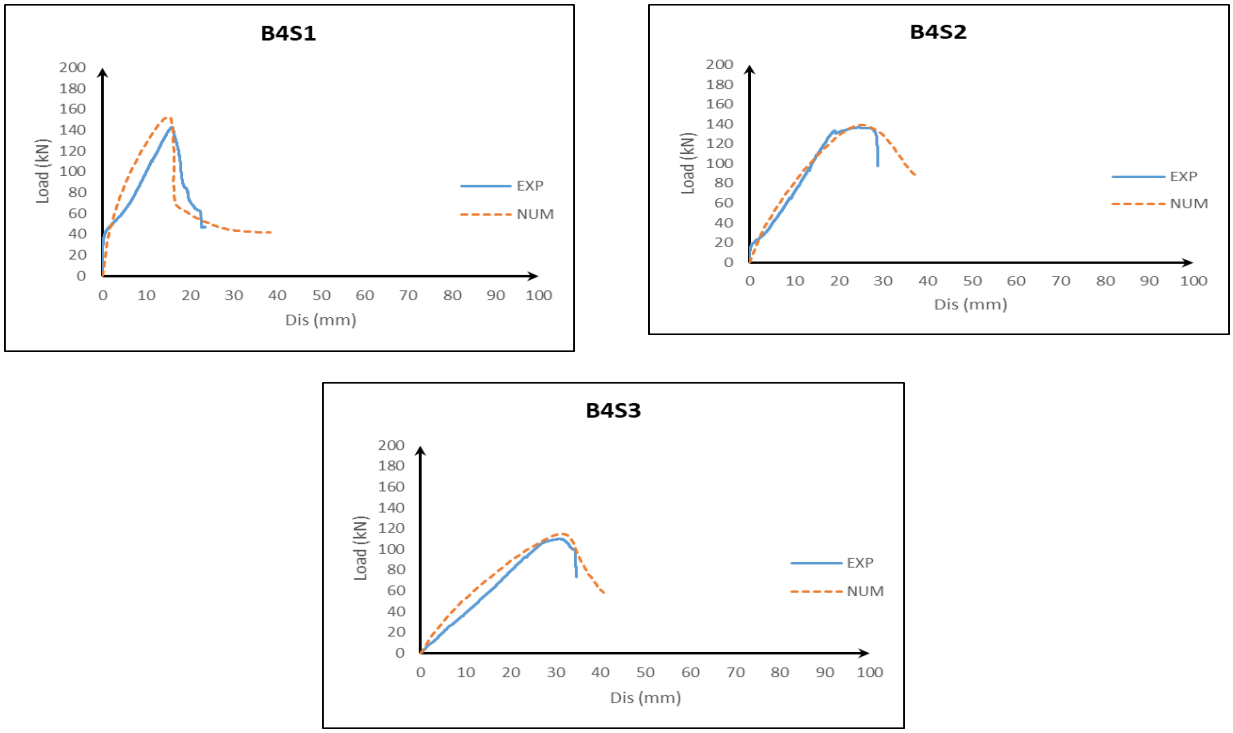

Figure 15. The load-deflection responses for third group both numerical and experimental

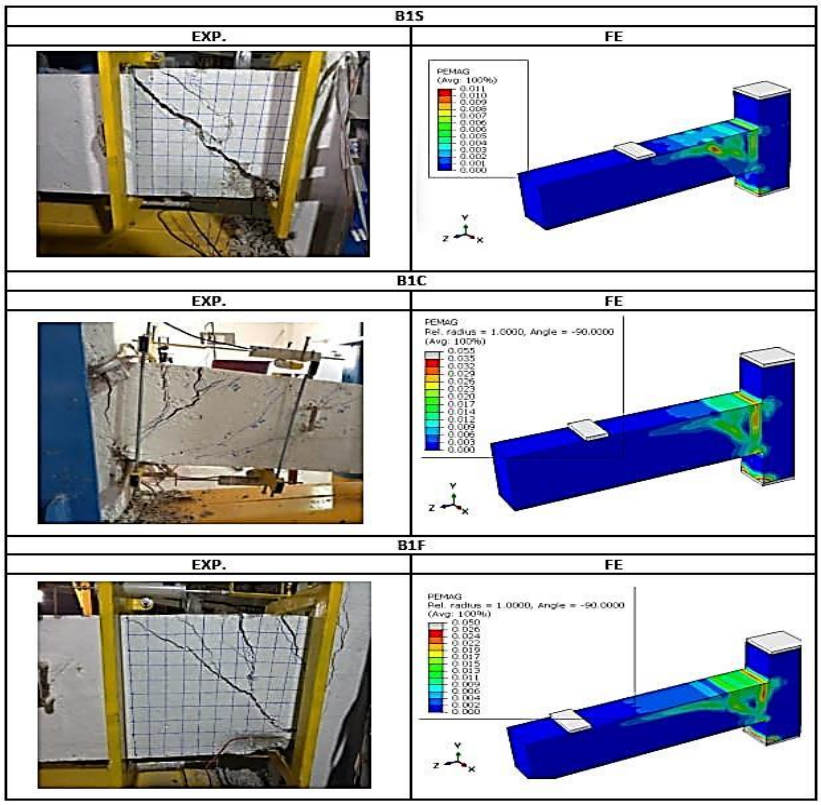

Figure 16. Failure modes of beams in first group obtained from numerical and experimental results

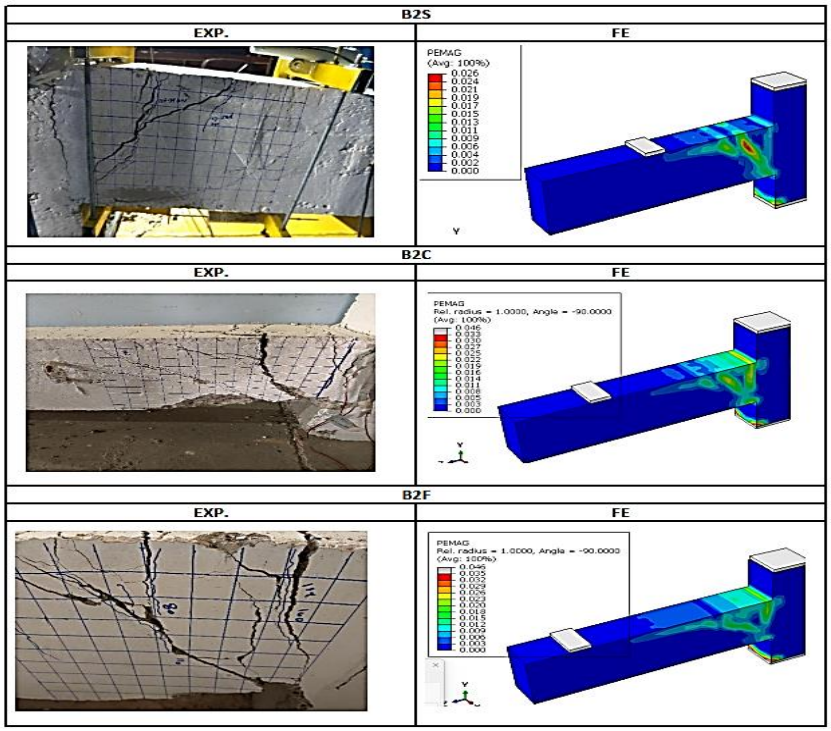

Figure 17. Failure modes of beams in second group obtained from numerical and experimental results

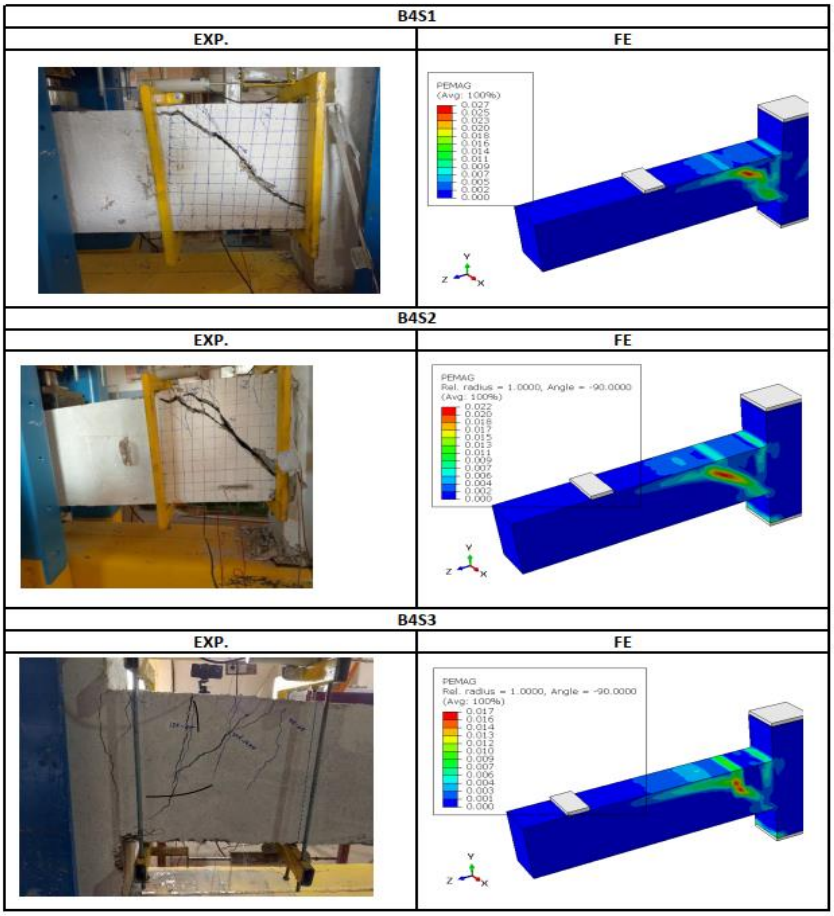

Figure 18. Failure modes of beams in third group obtained from numerical and experimental results

5. Conclusion

In the present study, experiments are carried out on RC beams with different shear reinforcement ratios and shear span-to-depth ratios. Measuring the components of shear strength that stirrups and concrete provide, Vs and Vc, respectively, is the goal. Additionally, the shear resistance of the RC beam at the first diagonal cracking, Vcr is to be determined. The test findings are evaluated by the authors through comparison with the projected values generated by various established models. The following deductions are made:

- In shear failure mode, the concrete contributes ranged between 74.7% and 87.3% of the total shear capacity of beams. In the combined failure mode, concrete contributes 34.8% to 75.6%.
- Larger spacing between stirrups leads to larger diagonal crack spacing, lowering beam load strength. Not all stirrups contribute equally to shear resistance;
- a ratio from 40% to 70% compared to beams without stirrups.
- The dowel action in the longitudinal reinforcement improves the distribution of shear forces, especially in beams with higher a/d ratios. The importance of the dowel action increases in beams that possess enough stirrup reinforcement.
- When it comes to general behaviour, failure mechanism, load deformation, and load capacity, the finite element analysis findings and the actual data were quite similar. This held true for beams with identical measurements, boundary circumstances (loading and supporting conditions), and material mechanical characteristics. The average discrepancy between the ultimate load capacity of the experiment and the prediction made by the ABAQUS computer model was 2.75 percent. The experimental and numerical results differed in deflection at ultimate loads by an average of 7.54%.

Notation

a = shear span
a/d = shear span-to-depth ratio
As = tensile steel
b = width of beam
d = effective cross-section depth
f'c = compressive concrete strength
fy = yield strength of tensile steel
s = spacing between stirrups
V = shear force
Vc = strength contribution by concrete
Vc exp = the calculated value of the concrete's strength contribution.
Vd = strength contribution by dowel action
Vs = strength contribution by stirrup
Vs. exp = calculated value of strength contribution by stirrup
φ = stirrup diameter
ρv = stirrup ratio
ρt = tensile steel ratio

References

[1] K. H. Reineck, E. C. Bentz, B. Fitik, D. A. Kuchma, and O. Bayrak, "ACI-DAfStb Database of Shear Tests on Slender Reinforced Concrete Beams without Stirrups," *ACI Structural Journal*, vol. 110, no. 5, 2013. https://doi.org/10.14359/51685839.

[2] K. H. Reineck, E. Bentz, B. Fitik, D. A. Kuchma, and O. Bayrak, "ACI-DAfStb Databases for Shear Tests on Slender Reinforced Concrete Beams with Stirrups," *ACI Structural Journal*, vol. 111, no. 5, 2014. https://doi.org/10.14359/51686627.

[3] K. H. Reineck and L. Todisco, "Database of Shear Tests for Non-Slender Reinforced Concrete Beams without Stirrups," *ACI Structural Journal*, vol. 111, no. 6, 2014. https://doi.org/10.14359/51687363.

[4] L. Todisco, K. H. Reineck, and O. Bayrak, "Database with shear tests on non-slender reinforced concrete beams with vertical stirrups," *ACI Structural Journal*, vol. 112, no. 6, pp. 761, 2015. https://doi.org/10.14359/51688127.

[5] D. E. Biskinis, G. K. Roupakias, and M. N. Fardis, "Degradation of shear strength of reinforced concrete members with inelastic cyclic displacements," *ACI Structural Journal*, vol. 101, no. 6, pp. 773-783, 2004. https://doi.org/10.14359/13426.

[6] fib-federation internationale du beton, *fib Model Code for Concrete Structures 2010*, John Wiley &

Sons, 2013. https://doi.org/10.1002/9783433604090.

[7] E. C. Bentz and M. P. Collins, "Development of the 2004 Canadian Standards Association (CSA) A23.3 shear provisions for reinforced concrete," *Canadian Journal of Civil Engineering*, vol. 33, no. 5, pp. 521-534, 2006. https://doi.org/10.1139/l06-006.

[8] H. Yokota, K. Rokugo, and N. Sakata, "JSCE recommendations for design and construction of high-performance fiber reinforced cement composite with multiple fine cracks," in *High Performance Fiber Reinforced Cement Composites*, vol. 2, Springer, Tokyo, Japan, 2008, pp. 761-770. https://doi.org/10.1007/978-90-481-3295-7_89.

[9] L. B. D. Specifications, *American Association of State Highway and Transportation Officials (AASHTO)*, Washington, DC, USA, 2012.

[10] T. C. Zsutty, "Beam shear strength prediction by analysis of existing data," *Journal Proceedings*, vol. 65, no. 11, pp. 943-951, Nov. 1968. https://doi.org/10.14359/6692.

[11] Z. P. Bazant and H. H. Sun, "Size effect in diagonal shear failure: influence of aggregate size and stirrups," *ACI Materials Journal*, vol. 84, no. 4, pp. 259-272, 1987. https://doi.org/10.14359/1510.

[12] M. N. Priestley, R. Verma, and Y. Xiao, "Seismic shear strength of reinforced concrete columns," *Journal of Structural Engineering*, vol. 120, no. 8, pp. 2310-2329, 1994. https://doi.org/10.1061/(ASCE)0733-9445(1994)120:8(2310).

[13] R. Medeot and T. Zordan, "Development and revision of the European Standard EN 15129 on anti-seismic devices," in *Life-Cycle Civil Engineering: Innovation, Theory and Practice*, CRC Press, 2021, pp. 600-608. https://doi.org/10.1201/9780429318294-73.

[14] K. K. Choi and H. G. Park, "Evaluation of inelastic deformation capacity of beams subjected to cyclic loading," *ACI Structural Journal*, vol. 107, no. 5, pp. 507, 2010. https://doi.org/10.14359/51663891.

[15] Q. M. Shakir and R. Alliwe, "Upgrading of deficient disturbed regions in precast RC beams with near surface mounted (NSM) steel bars," *Journal of Materials and Engineering Structures*, vol. 7, no. 2, pp. 167-184, 2020. https://doi.org/10.52925/jmes.v7i2.63.

[16] Q. M. Shakir and H. K. Hannon, "Innovative model of precast RC curved hybrid deep beams composed partially with high-performance concrete," *Arabian Journal for Science and Engineering*, vol. 49, no. 4, pp. 6045-6060, 2024. https://doi.org/10.1007/s13369-023-08195-6.

[17] M. W. Kani, M. W. Huggins, and R. R. Wittkopp, *Kani on Shear in Reinforced Concrete*, 1979.

[18] A. Muttoni and M. Fernández Ruiz, "Shear strength of members without transverse reinforcement as function of critical shear crack width," *ACI Structural Journal*, vol. 105, no. 2, pp. 163-172, 2008. https://doi.org/10.14359/19752.

[19] B. Hu and Y. F. Wu, "Effect of shear span-to-depth ratio on shear strength components of RC beams," *Engineering Structures*, vol. 168, pp. 770-783,2018. https://doi.org/10.1016/j.engstruct.2018.04.056.

[20] Y. Li, H. Chen, W. J. Yi, F. Peng, Z. Li, and Y. Zhou, "Effect of member depth and concrete strength on shear strength of RC deep beams without transverse reinforcement," *Engineering Structures*, vol. 241, p. 112427, 2021. https://doi.org/10.1016/j.engstruct.2021.112427.

[21] N. B., K. S. Abdul-Razzaq, and A. A. Hameed, "A parametric study on behavior of elliptical cantilever deep beams," 2022.

[22] Iraqi Specification No. 5, *Portland Cement*, Baghdad, 1984.

[23] Iraqi Specification No. 45, *Natural Sources for Gravel that is Used in Concrete and Construction*, Baghdad, 1984.

[24] T. O. Standard, *Standard Specification for Deformed and Plain Carbon Steel Bars for Concrete*, 2004.

[25] ASTM International, "ASTM C39M-14a: Standard test method for compressive strength of cylindrical concrete specimens," ASTM International,2014. https://doi.org/10.1520/C0039_C0039M-14A.

[26] ASTM International, "ASTM C78/C78M-16: Standard test method for flexural strength of concrete," 2016. https://doi.org/10.1520/C0078_C0078M-16.

[27] ASTM International, "ASTM D638-14: Standard test method for tensile properties of plastics," ASTM International, 2014. https://doi.org/10.1520/D0638-14.

[28] ASTM International, "ASTM D792-13: Standard test methods for density and specific gravity (relative density) of plastics by displacement," ASTM International, 2013. https://doi.org/10.1520/D0792-13.

[29] N. D. Koutas, "Experimental study on shear strength of RC beams using fiber reinforced polymer composites," Composite Structures, vol.

179, pp. 221-230, 2017. https://doi.org/10.1016/j.compstruct.2017.06.009.

[30] J. B. Fisher and C. W. Hwang, "The role of transverse reinforcement in shear strength of reinforced concrete beams," Journal of Structural Engineering, vol. 130, no. 7, pp. 1078-1089,2004. https://doi.org/10.1061/(ASCE)07339445(2004)130:7(1078).

[31] Y. Liu, L. Zhang, and Y. Sun, "Influence of transverse reinforcement on shear behavior of reinforced concrete beams," Engineering Structures, vol. 143, pp. 467-481, 2017. https://doi.org/10.1016/j.engstruct.2017.04.018.

[32] M. Y. Chen, Z. L. Xu, and L. X. Zhang, "Shear capacity of reinforced concrete beams with and without stirrups," Construction and Building Materials, vol. 95, pp. 230-240, 2015. https://doi.org/10.1016/j.conbuildmat.2015.07.046.

[33] F. L. Chung and J. Y. Wang, "Effect of shear span-to-depth ratio on shear strength and failure modes of concrete beams," Materials and Structures, vol. 53, no. 3, pp. 114-126, 2020. https://doi.org/10.1617/s11527-019-1404-2

[34] A. D. El-Tawil and A. E. H. El-Sayed, "Numerical analysis of shear strength in reinforced concrete beams using finite element methods," Structural Engineering and Mechanics, vol. 71, no. 4, pp. 437-448, 2019. https://doi.org/10.12989/sem.2019.71.4.437.

[35] Z. S. Park, T. J. He, and J. H. Lee, "Experimental investigation of shear behavior in reinforced concrete beams with different stirrup spacings," Journal of Civil Engineering and Management, vol. 21, no. 5, pp. 599-610, 2015. https://doi.org/10.3846/13923730.2014.973548.

[36] S. M. Smith and K. C. Ferris, "Shear strength of reinforced concrete beams: A review of experimental and theoretical studies," Structural Concrete, vol. 20, no. 2, pp. 175-190, 2019. https://doi.org/10.1002/suco.201800119.

[37] R. T. Shafieezadeh and A. M. Hassan, "Impact of transverse reinforcement on shear capacity of reinforced concrete beams: A review," Journal of Building Performance, vol. 11, no. 1, pp. 32-45, 2020. https://doi.org/10.3801/JBP.2020.11.1.32.

[38] I. Jelić, M. N. Pavlović, and M. D. Kotsovos, "A study of dowel action in reinforced concrete beams," Magazine of Concrete Research, vol. 51, no. 2, pp. 131-141, 1999. https://doi.org/10.1680/macr.1999.51.2.131.

[39] C. A. LaFave, "Comparative study of shear capacity models for concrete beams with various reinforcement types," Structural Engineering Review, vol. 12, no. 3, pp. 245-258, 2022. https://doi.org/10.1002/sen.2190.

[40] A. B. Ahmed and S. A. H. Zubair, "Behavior of reinforced concrete beams under cyclic loading: Experimental and numerical study," International Journal of Civil Engineering, vol. 18, no. 4, pp. 453-465, 2020. https://doi.org/10.1007/s40940-020-00118-3